

Dilution of dark matter relic density in singlet extension models

Yang Xiao,^{a,b} Jin Min Yang,^{a,b} Yang Zhang^{c,a}

^a*CAS Key Laboratory of Theoretical Physics, Institute of Theoretical Physics, Chinese Academy of Sciences, Beijing 100190, P. R. China*

^b*School of Physical Sciences, University of Chinese Academy of Sciences, Beijing 100049, P. R. China*

^c*School of Physics, Zhengzhou University, ZhengZhou 450001, P. R. China*

E-mail: xiaoyang@itp.ac.cn, jmyang@itp.ac.cn, zhangyangphy@zzu.edu.cn

ABSTRACT: We study the dilution of dark matter (DM) relic density caused by the electroweak first-order phase transition (FOPT) in the singlet extension models, including the singlet extension of the standard model (xSM), of the two-Higgs-doublet model (2HDM+S) and the next-to-minimal supersymmetric standard model (NMSSM). We find that in these models the entropy released by the strong electroweak FOPT can dilute the DM density to 1/3 at most. Nevertheless, in the xSM and NMSSM where the singlet field configuration is relevant to the phase transition temperature, the strong FOPT always happens before the DM freeze-out, making the dilution effect negligible for the current DM density. We derive an analytical upper bound on the freeze-out temperature and a numerical lower bound on nucleation temperature in the xSM. On the other hand, in the 2HDM+S where the DM freeze-out temperature is independent of FOPT, the dilution may salvage some parameter space excluded by excessive DM relic density or by DM direct detections.

Contents

1	Introduction	1
2	Dilution of DM density by first-order phase transition	3
2.1	Electroweak first-order phase transition	3
2.2	Dilution mechanism via entropy injection	4
2.3	DM relic density	5
3	Singlet extension of the SM	6
3.1	Effective potential	6
3.2	Scan results	9
3.2.1	Dilution factor	9
3.2.2	Constraints on dilution process	12
4	Singlet extension of two-Higgs-doublet model	14
5	Next-to-minimal supersymmetric standard model	16
6	Conclusions	17
	References	18

1 Introduction

The electroweak symmetry is broken in the present Universe, but is supposed to be restored in the early Universe [1]. In the Standard Model (SM), the electroweak symmetry-breaking occurs through a crossover transition [2], while it can be first-order phase transition (FOPT) in presence of Beyond-the-SM (BSM) physics. Studying of FOPT has been of heightened interest, because it could have provided the conditions needed for explanation of the baryon asymmetry of the Universe (BAU) [3–6] and generated detectable gravitational wave (GW) [7, 8].

The BAU is characterized by the baryon-to-entropy density ratio $Y_B \equiv n_B/s$ and the most precise measurement is given by Planck [9]

$$Y_B = 8.65 \pm 0.09 \times 10^{-11}, \quad (1.1)$$

which is consistent with the value obtained from measurements of primordial abundance for light elements [10]. The BSM physics to explain it must satisfy the so-called Sakharov criteria: C- and CP-violation, baryon number violation and departure from equilibrium [11]. Many mechanisms have been proposed following such criteria [3, 12–18]. The electroweak

baryogenesis is one of the most attractive scenarios and has been widely studied [3, 19–24], which requires an electroweak FOPT. The transition occurs when the bubbles of the symmetry-broken phase nucleate in plasma of the symmetry-restored phase. More baryons are produced than antibaryons in the regions around the expanding bubble walls. To avoid washing out the created baryons, the transition has to be strongly first-order.

The collisions, sound waves and turbulence from expanding bubbles of the broken phase can generate detectable GWs [25–27]. The observation of GW signal [28] has opened up a new window to probe BSM, especially in the situation that the LHC searches for BSM have merely given null results so far. The GW generated through strong FOPT is within coverage of future GW detectors, such as the Laser Interferometer Space Antenna (LISA) [29] and the Taiji program [30].

The other by-product of strong FOPT is the change of Dark Matter (DM) density. When the Universe evolved from the symmetric phase to the broken phase, there was an entropy injection and latent heat release, which could dilute the DM density. The DM relic density in the present Universe has been measured precisely by astrophysical and cosmological experiments: $\Omega_{\text{DM}}h^2 = 0.120 \pm 0.001$ [31]. The DM models, such as the Weakly Interacting Massive Particle (WIMP)[32–34], right hand neutrino [35–38] and axion[39–41], should give the correct relic density. Assuming a multi-component DM, the proportions of different DM candidates also affect the interpretation of DM direct and indirect searching results [42–44].

For those DM models in which the FOPT occurs after DM freeze-out in the evolution history of the Universe, it is mandatory to take the dilution of DM density into consideration. The dilution effect can be induced by the entropy injection, which may come from heavy states decaying to the thermal bath [45, 46] or the electroweak FOPT [47–52]. Refs. [47, 48] first showed some general information on the amounts of supercooling and reheating as well as the duration of the phase transition using thermodynamic method. Then in a model-independent way Ref. [49] found that the FOPT may dilute the thermal relic abundance of DM if the decouple process finished before the electroweak transition. Further, Ref. [50] systematically studied various imprints of the phase transitions on the relic abundance of TeV-scale DM. The above studies showed that the dilution factor, $d = (a_f/a_i)^3$ with $a_i(a_f)$ being the scale factor of the Universe at the beginning (ending) of the phase transition, can be as large as 50. It will distinctly affect the DM signal expectations in relevant experiments. However, the above studies focused on the dilution effect by using the toy-model-like effective potential such as adding large degree of freedom from hidden sector. In the studies of realistic models emphasizing DM aspect [53–57], the dilution effect has been neglected by a rough estimation.

In this work, we aim to study in detail the dilution of DM relic density caused by FOPT in realistic models. Therefore we focus on singlet extension models, including the scalar singlet extension of the SM (xSM), of two-Higgs-doublet model (2HDM+S) and the next-to-minimal supersymmetric Standard Model (NMSSM). These models are well motivated and popular in studying electroweak phase transition and DM. The introduced singlet can both trigger FOPT and provide a good DM candidate. We will calculate the magnitude of the dilution factor and find out the conditions of successful dilution of DM relic density in

these models.

This paper is organized as follows. In Sec. 2 we introduce the dilution mechanism caused by FOPT and deduce formulas for calculating the dilution factor. We describe the models and present results for xSM in Sec. 3, for 2HDM+S in Sec. 4, and for NMSSM in Sec. 5.

2 Dilution of DM density by first-order phase transition

2.1 Electroweak first-order phase transition

The amount of dilution on DM density depends upon the relative entropy injected into the broken phase during the FOPT. Two special temperatures of the FOPT, the critical temperature (T_c) and nucleation temperature (T_n) defined in the following, are the vital features in determining the dilution factor.

In the hot and radiation-dominated early Universe, the electroweak symmetry is restored, i.e. the minimum of Higgs potential locates at origin v_{origin} . As the temperature of the Universe drops, a second minimum v_{broken} away from the origin develops with higher free energy. With the Universe further cooling, the symmetry-broken minimum becomes degenerate with the origin, which gives the definition of critical temperature

$$V_{\text{eff}}(v_{\text{origin}}; T_c) = V_{\text{eff}}(v_{\text{broken}}; T_c). \quad (2.1)$$

Then, with temperature falling below T_c , some regions of the symmetric plasma tunnel to the deeper broken minimum and nucleate bubbles. Most of the bubbles are too small to grow and they just collapse, because the energy difference between the two vacuums is not large enough to overcome the surface tension of the bubble walls. As the Universe further cools, the nucleation rate of large bubbles increases dramatically. The phase transition begins once the probability to nucleate a supercritical bubble in one Hubble volume is of order one, at the so-called nucleation temperature T_n .

Quantitatively, the tunneling probability per unit time per unit volume can be roughly estimated as [58]

$$\Gamma \sim T^4 e^{-\frac{S_E}{T}}, \quad (2.2)$$

where S_E is the three-dimensional Euclidean action given by

$$S_E = 4\pi \int_0^{+\infty} r^2 dr \left[\frac{1}{2} \left(\frac{\partial \phi}{\partial r} \right)^2 + V_{\text{eff}}(\phi; T) \right]. \quad (2.3)$$

The bubble configuration $\phi(r)$ in the integral is fixed from the corresponding Euclidean equation of motion

$$\frac{d^2 \phi}{dr^2} + \frac{2}{r} \frac{d\phi}{dr} = \frac{\partial V_{\text{eff}}(\phi; T)}{\partial \phi}, \quad (2.4)$$

subjecting to the boundary conditions $\lim_{r \rightarrow \infty} \phi(r) = 0$ and $d\phi/dr|_{r=0} = 0$ (see [59] for details). The $\mathcal{O}(1)$ probability of nucleating a supercritical bubble in one Hubble volume is expressed as

$$\int_{T_n}^{+\infty} \frac{dT}{T} \left(\frac{2\zeta M_{Pl}}{T} \right)^4 e^{-\frac{S_E}{T}} = \mathcal{O}(1), \quad (2.5)$$

where M_{PL} is the reduced Planck mass, $\zeta = \frac{1}{4\pi} \sqrt{\frac{45}{\pi g^*}}$ with g^* being the effective number of relativistic degrees of freedom [60]. From this definition, we can get an estimated formula for T_n

$$\frac{S_E}{T_n} \sim \mathcal{O}(130 - 140). \quad (2.6)$$

2.2 Dilution mechanism via entropy injection

There are two situations for the dilution of DM density due to entropy injection. In the first situation, the transition temperature T_n is near the critical temperature T_c , and the supercooling process is negligible. The system is almost in equilibrium and thus the total entropy ($\sim a^3 s$) is conserved, where s indicates the entropy density and a is the scale factor of the Universe. With entropy injection, the density changes as $s_- = (a_i/a_f)^3 s_+$, where the subscripts $+$ and $-$ denote the high-temperature symmetric phase and low-temperature broken phase, and the subscripts f and i indicate the beginning and ending of the phase transition. Therefore we can get the dilution factor

$$d \equiv \left(\frac{a_f}{a_i}\right)^3 = \frac{s_+(T_c)}{s_-(T_n)}, \quad (2.7)$$

for the transition in this situation.

In the second situation, where the transition is strongly first-order and T_n is consequently much smaller than T_c , the equilibrium condition is broken at a stage of the transition. For convenience, we can divide the evolution of transition into supercooling stage, reheating stage and phase coexistence stage.

In the supercooling stage, the high temperature phase always dominates the Universe, so the total entropy is conserved. Similar to the first situation, we have

$$\left(\frac{a_i}{a_m}\right)^3 \simeq \frac{s_+(T_n)}{s_+(T_c)}, \quad (2.8)$$

where a_m is the scale factor at a temperature near T_n , corresponding to the end of supercooling.

Then the latent heat is released and reheats the Universe. If the duration of the reheating stage is short compared to the expansion rate, the energy density ρ , instead of the total entropy, is conserved [49]. When the Universe is reheated to a temperature close to T_c , it reaches a phase coexistence stage, and its energy density can be expressed as

$$\rho_-(T_c) = f\rho_-(T_c) + (1-f)\rho_+(T_c), \quad (2.9)$$

where f is the volumetric fraction of the plasma of the low-temperature phase. With energy density conservation, the energy density at the beginning of the reheating stage is given as

$$\begin{aligned} \rho_+(T_n) &= \rho_-(T_c) \\ &= \rho_+(T_c) - f[\rho_+(T_c) - \rho_-(T_c)]. \end{aligned} \quad (2.10)$$

Then we can get the fraction

$$f = \frac{\rho_+(T_c) - \rho_+(T_n)}{L}, \quad (2.11)$$

where $L = \rho_+(T_c) - \rho_-(T_c)$ is the latent heat.

During the third stage, which also happens quickly, the total entropy is again conserved. The total entropy is approximately $a_m^3 [(1-f)s_+(T_c) + fs_-(T_c)]$ at the beginning and $a_f^3 s_-(T_c)$ at the ending of this stage. Therefore we see

$$\left(\frac{a_f}{a_m}\right)^3 = \frac{1 - f\Delta s/s_+(T_c)}{1 - \Delta s/s_+(T_c)}, \quad (2.12)$$

where $\Delta s = s_+(T_c) - s_-(T_c)$. Finally, combined with Eq. (2.8), we get the total expansion of dilution factor

$$d \equiv \left(\frac{a_f}{a_i}\right)^3 = \left(\frac{1 - f\Delta s/s_+(T_c)}{1 - \Delta s/s_+(T_c)}\right) \left(\frac{s_+(T_c)}{s_+(T_n)}\right). \quad (2.13)$$

for the second situation.

2.3 DM relic density

The relic density of freeze-out DM is calculated through solving the Boltzmann transport equation [61]

$$\frac{dn_{\text{DM}}}{dt} = -3Hn_{\text{DM}} - \langle v_{\text{rel}}\sigma \rangle (n_{\text{DM}}^2 - n_{\text{DM,eq}}^2), \quad (2.14)$$

where n_{DM} is the DM number density, $n_{\text{DM,eq}}$ is the DM number density at thermal equilibrium with the rest of the universe, H is the Hubble rate and $\langle v_{\text{rel}}\sigma \rangle$ is the relative velocity of the annihilating DM particles times the thermally averaged self-annihilation cross-section. This equation states that the change of the DM density comes from two parts: (1) the dilution effect due to Hubble expansion, (2) the particle reactions including DM production and DM annihilation. Trading n_{DM} and t with $Y = n_{\text{DM}}/T^3$ and $x = m_{\text{DM}}/T$ respectively, the Boltzmann equation becomes the Riccati equation

$$\frac{dY}{dx} = -\frac{\lambda}{x}(Y^2 - Y_{\text{eq}}^2), \quad (2.15)$$

where

$$\lambda = \sqrt{\frac{45}{4\pi^3 g_*}} m_{\text{DM}} M_p \langle v_{\text{rel}}\sigma \rangle. \quad (2.16)$$

By dimensional analysis, the magnitude is estimated as $\lambda = 1.59 \times 10^8 \mathcal{F}/g_*(m_{\text{DM}}/1 \text{ GeV})^3$, where \mathcal{F} is a fudge factor to take account of the number of annihilation channels and the details of the interaction responsible for the annihilation [62, 63]. Treating λ as a constant number, we can solve the Riccati equation numerically with certain boundary conditions, such as shown in Fig. 1.

At high temperature, we have $x = m_{\text{DM}}/T \ll 1$ and $\lambda/x \gg 1$, so there is a strong negative feedback effect on Y . Any deviation with respect to Y_{eq} will lead to an opposite derivative in the right side of Eq. (2.15), and thus Y remains at Y_{eq} at high temperatures. When the universe cools down below the DM mass, Y_{eq} will decrease exponentially as e^{-x} , so does Y . Finally, when the temperature is much lower than the DM mass, i.e. below the so-called freeze-out temperature $T_f = m_{\text{DM}}/x_f$, λ/x is so small that the DM deviates from the thermal equilibrium and Y turns to a constant, which corresponds to the DM relic density.

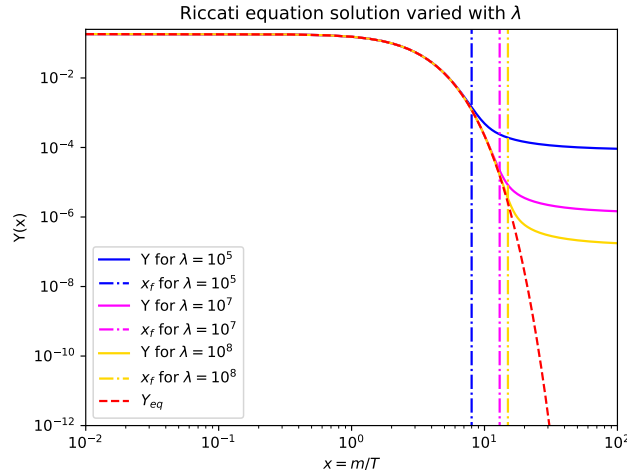


Figure 1. The solution of the Riccati equation with varying λ . The red dashed line shows the Y_{eq} at the thermal equilibrium. The blue, pink and yellow solid line are Riccati solution when $\lambda = 10^5, 10^7, 10^8$, respectively.

The dilution effect caused by FOPT can alter the curves of $Y(x)$ displayed in Fig. 1. If the freeze-out temperature is higher than the transition temperature, there will be a drop at $x = m_{DM}/T_n > x_f$ in the flat region, whose magnitude is decided by the dilution factor in Eq. 3.18. Thus, the final DM density can be calculated using the transitional method and then multiplying by the dilution factor d . However, in the numerical tools such as `MicrOmega` [64] and `MadDM` [65], the DM mass and couplings in the Boltzmann equation are set to the values with spontaneous symmetry breaking at zero-temperature, which is fine when $T_n > T_f \sim 0$ GeV. In our case, the DM mass should be calculated in the electroweak symmetry restored vacuum with thermal corrections. Fortunately, we see in Fig. 1 that the freeze-out temperature T_f does not change too much with λ varying in a large range. Therefore, in the following, we still estimate the DM relic density using `MicrOmega`, and leave the sophisticated calculation for future work. On the other hand, if $T_n > T_f$, the drop will happen on the left side of x_f . Owing to the strong negative feedback effect on Y in Eq. (2.15), the value of x_f is barely changed, as well as the DM relic density.

3 Singlet extension of the SM

3.1 Effective potential

Firstly, we consider xSM, the simplest scalar extension of the SM, which includes an extra Z_2 symmetric real scalar singlet field S . The scalar potential is given by

$$V_0(H, S) = -\mu_H^2 H^\dagger H + \lambda_H (H^\dagger H)^2 - \frac{\mu_S^2}{2} S^2 + \frac{\lambda_S}{4} S^4 + \frac{\lambda_{HS}}{2} H^\dagger H S^2. \quad (3.1)$$

The Higgs doublet can be parameterized as

$$H = \begin{bmatrix} G^+ \\ \frac{h+iG^0}{\sqrt{2}} \end{bmatrix}, \quad (3.2)$$

where $G^{\pm,0}$ indicate the Goldstone bosons and h stands for the SM Higgs boson. We parameterize the S field as $S = s$. The background field configurations h and s have vacuum expectation values (VEVs) of (v_h, v_s) at zero-temperature. Substituting them into Eq (3.1), the tree level tadpole conditions are

$$\begin{aligned}\left\langle \frac{\partial V_0}{\partial h} \right\rangle &= v_h \left(-\mu_H^2 + \lambda_H v_h^2 + \frac{\lambda_{HS}}{2} v_s^2 \right) = 0, \\ \left\langle \frac{\partial V_0}{\partial s} \right\rangle &= v_s \left(-\mu_S^2 + \lambda_S v_s^2 + \frac{\lambda_{HS}}{2} v_h^2 \right) = 0,\end{aligned}\tag{3.3}$$

where $\langle \dots \rangle$ represents that the quantity in between the angled brackets is evaluated in the vacuum ($h = v_h, s = v_s$). Among the solutions of Eq. (3.3), we take the Z_2 invariant one, $v_h = \mu_H^2/\lambda_H$ and $v_s = 0$. The scalar masses are obtained by diagonalizing the squared mass matrix evaluated at the VEV,

$$\begin{aligned}M^2 &= \begin{pmatrix} \left\langle \frac{\partial^2 V_0}{\partial h^2} \right\rangle & \left\langle \frac{\partial^2 V_0}{\partial h \partial s} \right\rangle \\ \left\langle \frac{\partial^2 V_0}{\partial h \partial s} \right\rangle & \left\langle \frac{\partial^2 V_0}{\partial s^2} \right\rangle \end{pmatrix} \\ &= \begin{pmatrix} 3v_h \lambda_H - \mu_H^2 + \frac{1}{2} \lambda_{HS} v_s^2 & \lambda_{HS} v_h v_s \\ \lambda_{HS} v_h v_s & 3v_s \lambda_S - \mu_S^2 + \frac{1}{2} \lambda_{HS} v_h^2 \end{pmatrix}.\end{aligned}\tag{3.4}$$

Since $v_s = 0$, the off-diagonal elements of the mass matrix are eliminated, i.e. no mixing between the Higgs and singlet fields. Owing to this, the singlet scalar particle does not interact with any other particles except the Higgs boson, which consequently is a viable DM candidate.

The relic density of this DM candidate is mainly determined by Higgs funnel annihilation. The cross section for annihilation into SM particles except Higgs is [66]

$$\sigma v_{\text{rel}} = \frac{2\lambda_{hs}^2 v_h^2}{\sqrt{s}} \frac{\Gamma_h(\sqrt{s})}{(s - m_h^2)^2 + m_h^2 \Gamma_h^2(m_h)},\tag{3.5}$$

where $\Gamma_h(m_h^*)$ is the full Higgs boson width as a function of invariant mass. Its thermal average is given as [67]

$$\langle \sigma v_{\text{rel}} \rangle = \int_{4m_S^2}^{\infty} \frac{\mathbf{s} \sqrt{\mathbf{s} - 4m_S^2} K_1(\sqrt{\mathbf{s}/T}) \sigma v_{\text{rel}}}{16T m_S^4 K_2^2(m_S/T)} d\mathbf{s},\tag{3.6}$$

where K_1 and K_2 are the second kind modified Bessel functions. As the annihilation is via the s -wave, the relic density can be estimated as

$$\Omega_S h^2 \sim \frac{3 \times 10^{-27} \text{cm}^3/\text{s}}{\langle \sigma v_{\text{rel}} \rangle} \times d,\tag{3.7}$$

if the freeze-out temperature is higher than the transition temperature.

To calculate the dilution factor of phase transition, we need the effective potential with loop corrections

$$V_{\text{eff}}(h, s; T) = V_0(h, s) + V_{\text{CW}}(h, s) + V_{\text{CT}}(h, s) + V_{1T}(h, s; T) + V_{\text{ring}}(h, s; T),\tag{3.8}$$

where V_{CW} , V_{CT} , V_{1T} and V_{ring} are the one-loop Coleman-Weinberg potential, the corresponding counter term, the one-loop thermal correction and the resummed daisy correction, respectively.

We choose the OS-like scheme and the Landau gauge to avoid introducing dependence on renormalization scale [60]. The one-loop zero-temperature correction takes a form [19]

$$V_1(h, s) = V_{\text{CW}}(h, s) + V_{\text{CT}}(h, s) \\ = \sum_i (-1)^{s_i} \frac{g_i}{64\pi^2} \left\{ m_i^4(h, s) \left[\log \frac{m_i^2(h, s)}{m_i^2(v_h, v_s)} - \frac{3}{2} \right] + 2m_i^2(h, s)m_i^2(v_h, v_s) \right\}, \quad (3.9)$$

where $i \in \{H, S, W^\pm, Z, \gamma, t\}$, s_i is the spin of particle i , and g_i is the number of degrees of freedom,

$$g_H = 1, \quad g_S = 1, \quad g_{W^\pm} = 6, \quad g_Z = 3, \quad g_\gamma = 3, \quad g_t = 12. \quad (3.10)$$

$m_i^2(h, s)$ stands for the squared tree-level background-field-dependent masses,

$$m_H^2 = -\mu_H^2 + 3\lambda_H h + \frac{1}{2}\lambda_{HS}s^2 \\ m_S^2 = -\mu_S^2 + 3\lambda_S s + \frac{1}{2}\lambda_{HS}h^2 \\ m_{W^\pm} = \frac{1}{4}g_{SU(2)_L}^2 h^2, \quad m_Z = \frac{1}{4} \left(g_{SU(2)_L}^2 + g_{U(1)_Y}^2 \right) h^2 \\ m_\gamma = 0, \quad m_t = \frac{1}{2}y_t^2 h^2. \quad (3.11)$$

We neglect the contributions of light fermions. Goldstone bosons are not included because that second derivative of V_{CW} is logarithmic divergent at VEV of zero-temperature, originating from $m_{G^{\pm,0}}|_{h=v_h, s=0} = 0$ and $\partial m_{G^{\pm,0}}/\partial h|_{h=v_h, s=0} \neq 0$ [68]. The impact of fixing the Goldstone catastrophe, as well as choosing other renormalization scheme, can be found in Ref. [69, 70].

In the OS-like scheme, the position of VEV at zero-temperature and masses at VEV are not affected by loop corrections, so the renormalization conditions are imposed as

$$\left\langle \frac{\partial(V_0 + V_1)}{\partial h} \right\rangle = \left\langle \frac{\partial V_0}{\partial h} \right\rangle = 0, \\ \left\langle \frac{\partial^2(V_0 + V_1)}{\partial^2 h} \right\rangle = \left\langle \frac{\partial^2 V_0}{\partial^2 h} \right\rangle = m_H^2, \quad \left\langle \frac{\partial^2(V_0 + V_1)}{\partial^2 s} \right\rangle = \left\langle \frac{\partial^2 V_0}{\partial^2 s} \right\rangle = m_S^2. \quad (3.12)$$

Thus, with $v_h = 246$ GeV and $m_H = 125$ GeV, we can fix μ_H with Eqs. (3.3) and (3.4). We choose m_S , λ_S and λ_{HS} as input parameters of the model.

The one-loop finite temperature correction is deduced from the finite-temperature field theory [60]

$$V_{1T}(h, s) = \frac{T^4}{2\pi^2} \left[\sum_B g_B J_B \left(\frac{m_B(h, s)}{T} \right) + \sum_F g_F J_F \left(\frac{m_F(h, s)}{T} \right) \right], \quad (3.13)$$

where J_B , J_F are the relevant thermal distribution functions for the bosonic and fermionic contributions, respectively,

$$J_{B,F}(x) = \pm \int_0^{+\infty} dy y^2 \log \left(1 \mp e^{-\sqrt{x^2+y^2}} \right). \quad (3.14)$$

In the high-temperature limit, they can be expanded as

$$\begin{aligned} J_B(x) &= -\frac{\pi^4}{45} + \frac{\pi^2}{12}x^2 - \frac{\pi}{6}x^3 - \frac{x^4}{32}\log\frac{x^2}{a_b}, \\ J_F(x) &= -\frac{7\pi^4}{360} + \frac{\pi^2}{24}x^2 + \frac{x^4}{32}\log\frac{x^2}{a_f}, \end{aligned} \quad (3.15)$$

where $\log(a_b) = \frac{3}{2} - 2\gamma + 2\log(4\pi)$, $\log(a_f) = \frac{3}{2} - 2\gamma + 2\log(\pi)$, with γ being the Euler constant [19].

Owing to the zero-mode contribution, the multi-loop diagrams will dominate if the temperature is high enough, which makes the perturbation condition broken [71, 72]. To make the expansion reliable, the dominant thermal pieces must be resummed. Here we adopt the Parwani method [73] by replacing the tree-level masses m_i^2 in Eqs. (3.9) and (3.13) through the thermal masses $m_i^2(T) = m_i^2 + d_i T^2$, where $d_i T^2$ is the leading contribution in temperature to the one-loop thermal mass, where

$$\begin{aligned} d_{W^{\pm,3}}^L &= \frac{11}{6}g_{SU(2)_L}^2, & d_{W^{\pm,3}}^T &= 0, & d_B^L &= \frac{11}{6}g_{U(1)_Y}^2, \\ d_{HH} &= \frac{3g_{SU(2)_L}^2}{16} + \frac{1}{16}g_{U(1)_Y}^2 + \frac{1}{2}\lambda_H + \frac{1}{4}y_t^2 + \frac{1}{24}\lambda_{HS}, \\ d_{SS} &= \frac{1}{4}\lambda_S + \frac{1}{6}\lambda_{HS}. \end{aligned} \quad (3.16)$$

3.2 Scan results

We performed a scan in the following ranges,

$$10 \text{ GeV} \leq m_S \leq 1 \text{ TeV}, \quad 0 \leq \lambda_{HS} \leq 10, \quad 0 \leq \lambda_S \leq 1. \quad (3.17)$$

The upper bounds on λ_S and λ_{HS} are set because of perturbation limits. We will see later that the upper bound on m_S is large enough for achieving strong FOPT. `CosmoTransition` [74] and `PhaseTracer` [75] are used to calculate the physical quantities related to the phase transition, and `MicrOmega` is used to get the freeze-out temperature T_f and DM observables. In the following, we study samples that can achieve successfully FOPT in the thermal history of the Universe. The bound on DM relic density from Planck [9] and limits from DM direct detection XENON1T [44] are discussed later taking the dilution effect into consideration. For other possible constraints on xSM, see Refs. [76].

3.2.1 Dilution factor

The top left panel of Fig. 2 displays the results of the dilution factor as a function of the model parameters. It finds that the dilution effect can be neglected in most of the parameter space that can achieve FOPT, except at the upper edge on (m_s, λ_{hs}) plane. In the upper edge, the phase transition happens mostly between minimums of $(v_h^{\text{high}} = 0, v_s^{\text{high}} \neq 0)$ and $(v_h^{\text{low}} \neq 0, v_s^{\text{low}} = 0)$, which is strong first-order and corresponds to a large difference between T_c and T_n . It can be seen from the top panels of Fig. 2, the larger the difference is, the more obvious the dilution is. This is consistent with the results in previous studies that the dilution can be neglected when $T_c \sim T_n$ [53, 54], and is significant if supercooling

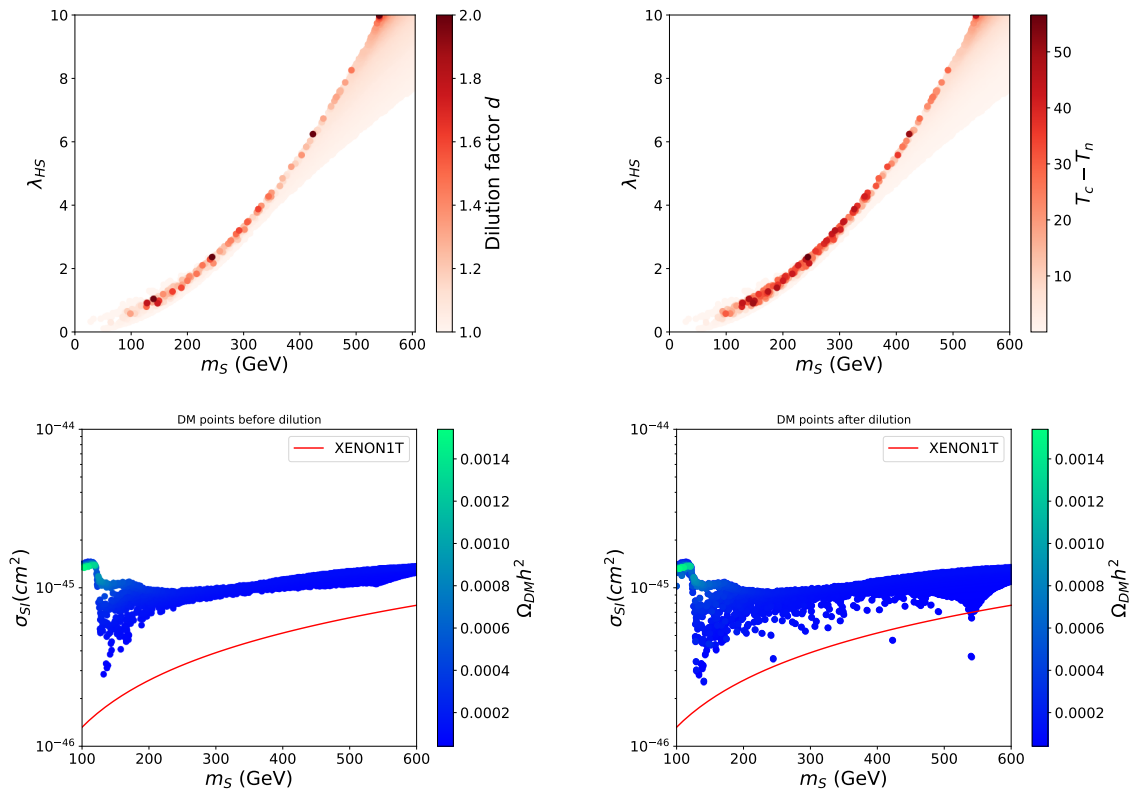


Figure 2. **Top:** the dilution factor (left) and supercooling information (right) in the plane of input parameters. **Bottom:** the cross section of spin-independent scattering of DM on nucleon without (left) and with (right) dilution of DM relic density caused by FOPT taken into consideration, along with the 90% CL limit from XENON1T.

occurs [48, 49]. The impact of supercooling can be expected from Eq. (2.13). At high temperatures, the dominant part of effective potential is the quartic term of temperature provided by Eq (3.13). Thus the dilution factor can be estimated as

$$s = -\frac{dV_{\text{eff}}}{dT}, \quad \left(\frac{a_f}{a_i}\right)^3 \sim \left(\frac{T_c}{T_n}\right)^3 \sim \left(1 + \frac{\Delta}{T_n}\right)^3. \quad (3.18)$$

In the bottom panels of Fig. 2, we present the cross section of spin-independent scattering of DM on nucleon for the above samples, along with the 90% CL limit from XENON1T [44]. In the case of singlet DM relic density $\Omega_S h^2$ smaller than the observed value $\Omega_{\text{DM}} h^2 = 0.120$, which means that the singlet DM is only a fraction of DM, we rescale the cross section by a factor of $f_{\text{rel}} = \Omega_S / \Omega_{\text{DM}}$. The bottom panels show the results without and with the dilution of $\Omega_S h^2$. One can see that the dilution can salvage some samples excluded by DM direct detection. This is the reason why the dilution caused by FOPT should be taken into consideration in DM studies.

The largest value of the dilution factor in our scan is 2.8, which may be raised a little with more sophisticated scan. However, as it is correlated with the difference $T_c - T_n$, we find that it is hard to obtain a dilution factor larger than 3. In Fig. 3 we displace T_c ,

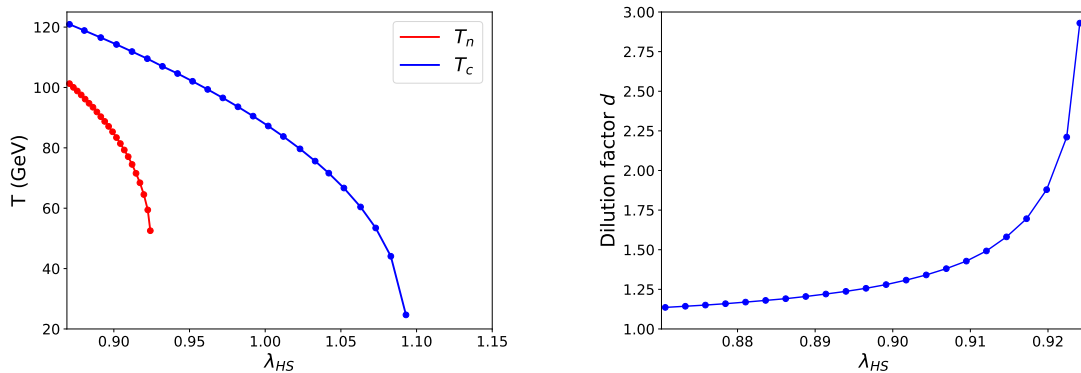


Figure 3. The critical temperature T_c , the nucleation temperature T_n and the dilution factor d as functions of the input parameter λ_{HS} , with fixed $m_s = 129.5070$ GeV and $\lambda_S = 0.5286$.

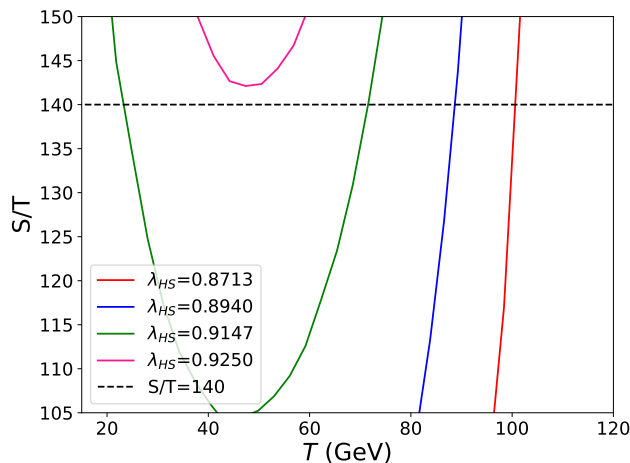


Figure 4. The ratio of the Euclidean action to the temperature S/T versus the temperature for different λ_{HS} values. Other input parameters are same as in Fig. 3.

T_n and the dilution factor d as functions of the model parameter λ_{HS} for a benchmark point with $m_s = 129.5070$ GeV and $\lambda = 0.5286$. We see in the left panel that the critical temperature T_c and the nucleation temperature T_n both decrease but with different speeds as λ_{HS} increases. Theoretically, the lowest value of T_c can reach to zero by fine tuning the parameter λ_{HS} , as discussed in Ref. [70]. However, the nucleation temperature has a lower bound around 50 GeV. The reason of existing this lower bound is displaced in Fig. 4, where the colored solid curves indicate the ratio of the Euclidean action to the temperature as functions of the temperature for different λ_{HS} values. The nucleation temperature is obtained from condition $S/T = 140$, namely the intersection of the colored curves and the horizontal black dashed line. With λ_{HS} increasing, the intersection moves to the left and the slope of S/T decrease. When $\lambda_{HS} > 0.9250$, the S/T curve looks U-shaped and there is no more intersection with the horizontal line, which means that the FOPT can not finish

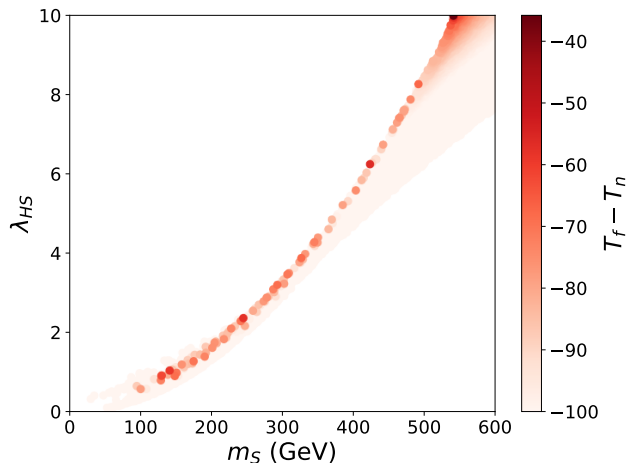


Figure 5. The difference between DM freeze-out temperature T_f and the nucleation temperature T_n in the plane of input parameters.

in the history of the Universe.

The difference between T_c and T_n increases with λ_{HS} increasing as well, and stops at about 50 GeV because of no nucleation temperature for larger λ_{HS} . Therefore, the dilution factor increases with increasing λ_{HS} and has an upper bound about 3 for this benchmark point, as shown in the right panel of Fig. 3.

3.2.2 Constraints on dilution process

Although the dilution in xSM is sizable to affect DM properties, there are two essential prerequisites in the calculation of dilution factor described in Sec. 2. In the case of supercooling the liberated latent heat reheats the system back to a temperature close to T_c , and the phase transition happens after the singlet DM freeze-out. Now we check the two conditions for the above scan result.

In Eq. (2.9), the volumetric fraction of the low temperature phase during the reheating stage f must be smaller than 100%. However, using Eq. (2.11), it can exceed 100% especially for samples of large dilution factor. It is because Eq. (2.11) assumes that a large amount transition latent heat brings temperature of the system from T_n back to near T_c , which fails when $T_c \gg T_n$. In this case, T_n appearing in Eq. (2.13) should be replaced by reheating temperature T_r . The calculation of T_r involves processing specific kinetic processes [48], which is out of the scope of this paper. Neglecting the term including f , i.e. setting $f = 100\%$, Eq. (2.13) approaches to Eq. (3.18) and gives a larger dilution factor. Moreover, friction and collisions in the walls of bubbles would also release entropy and increase the dilution [49], which are not included in Eq. (2.13). Thus, breaking of this assumption does not indicate reduction of dilution factor.

As for the second prerequisite, in order to avoid the DM reequilibrate with other thermal species, the nucleation temperature T_n shall be smaller than the singlet DM freeze-out temperature T_f . As discussed in Fig. 4, there is a lower bound on T_n , and the lowest T_n

in our scan is about 50 GeV. On the other hand, the variable $x_f = m_S/T_f$ used in solving the Boltzmann transport equation of matter lies in range of $\mathcal{O}(20 \sim 40)$ in xSM. We see from Fig. 2 that m_S is smaller than 600 GeV when $d > 1.5$ and $\lambda_{HS} < 10$, which indicates $T_f < 30 \text{ GeV} < T_n$, i.e. the dilution process happens before the DM freeze-out and can not affect the current singlet DM density. This can be seen from Fig. 5 which shows that for the samples of FOPT the DM freeze-out temperature is always lower than the nucleation temperature. The mass of singlet DM is bounded because large dilution factor requires transition between minimums $(0, v_s^{\text{high}} \neq 0)$ and $(v_h^{\text{low}} \neq 0, 0)$. The upper bound can be estimated using high temperature approximation.

Using Eq. (3.15) and neglecting the zero-temperature corrections and the finite temperature corrections beyond T^2 terms, we can get the approximate effective potential [77]

$$V_{\text{HT}}(h, s; T) = \frac{1}{2}(-\mu_H^2 + c_H T^2)h^2 + \frac{1}{4}\lambda_H h^4 + \frac{1}{2}(-\mu_S^2 + c_S T^2)s^2 + \frac{1}{4}\lambda_S s^4 + \frac{1}{4}\lambda_{HS} h^2 s^2, \quad (3.19)$$

where

$$\begin{aligned} c_S &= \frac{2\lambda_{HS} + 3\lambda_S}{12}, \\ c_H &= \frac{9g_{SU(2)_L}^2 + 3g_{U(1)_Y}^2 + 12y_t^2 + 24\lambda_H + 2\lambda_{HS}}{48}. \end{aligned} \quad (3.20)$$

In order to obtain FOPT between minimums

$$\left(0, v_s^{\text{high}} = \frac{-\mu_S^2 + c_S T^2}{\lambda_S} \neq 0\right) \quad \text{and} \quad \left(v_h^{\text{low}} = \frac{-\mu_H^2 + c_H T^2}{\lambda_H} \neq 0, 0\right), \quad (3.21)$$

with temperature decreasing from high value, v_s^{high} must become non-zero before v_h^{low} become non-zero. It gives

$$\frac{\mu_H^4}{c_H^2} < \frac{\mu_S^4}{c_S^2}. \quad (3.22)$$

On the other hand, $(v_h^{\text{low}}, 0)$ must be deeper than $(0, v_s^{\text{high}})$ when $T < T_c$, such as $T = 0$ at zero-temperature minimum, which implies

$$\frac{\mu_H^4}{\lambda_H} > \frac{\mu_S^4}{\lambda_S}. \quad (3.23)$$

Combining the two constraints, we can obtain

$$\frac{\mu_H^4}{c_H^2} c_S^2 < \mu_S^4 < \frac{\mu_H^4}{\lambda_H} \lambda_S \rightarrow \frac{\mu_H^2}{c_H} c_S < \mu_S^2 < \frac{\mu_H^2}{\sqrt{\lambda_H}} \sqrt{\lambda_S}. \quad (3.24)$$

Note that μ_S^2, μ_H^2 are positive. Then recalling $\mu_S^2 = \lambda_{HS} \frac{v_h^2}{2} - m_S^2$, the constrain on m_S reads

$$\frac{-\mu_H^2}{\sqrt{\lambda_H}} \sqrt{\lambda_S} + \lambda_{HS} \frac{v_h^2}{2} < m_S^2 < \frac{-\mu_H^2}{c_H} c_S + \lambda_{HS} \frac{v_h^2}{2}. \quad (3.25)$$

In Fig. 6, we display the upper bound and lower bound on m_S for $\lambda_S = 0.1$ and $\lambda_S = 1$ with varying λ_{HS} . The upper bound and lower bound meet in a point, i.e. maximal value of m_S . Taking perturbation limits on λ_S and λ_{HS} into consideration, there is no way that

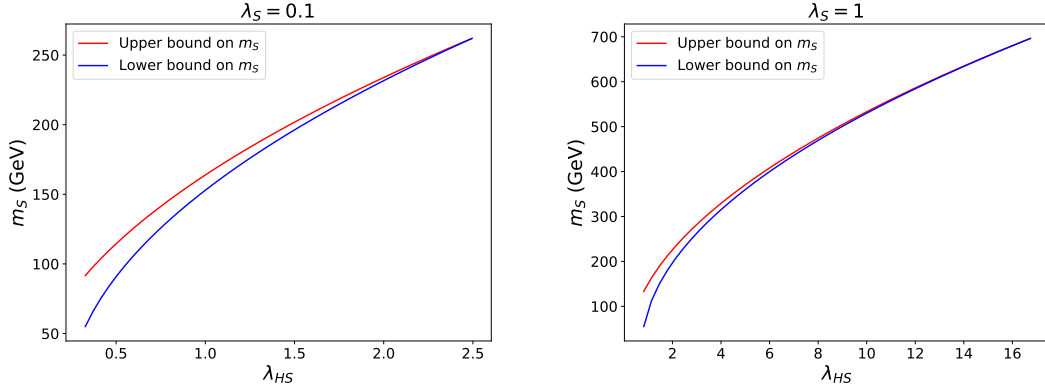


Figure 6. The lower and upper bounds on m_S obtained from high-temperature approximated potential for transition between $(0, v_s^{\text{high}} \neq 0)$ and $(v_h^{\text{low}} \neq 0, 0)$.

m_S in Eq. (3.25) exceeds 600 GeV. Even without perturbation limits, it is hard to obtain $m_S > 1$ TeV, namely $T_f > 50$ GeV.

By and large, the phase transition always happens after the singlet DM freeze-out in xSM, because the strong FOPT and the perturbation limits set an upper bound of 30 GeV on T_f , while the lowest T_n is above 50 GeV. The dilution of the current singlet DM density in the xSM can be neglected.

4 Singlet extension of two-Higgs-doublet model

Since the obstacle to achieve the dilution of DM relic density in the xSM is the mass upper bound on the singlet DM, we now turn to the singlet extension of the 2HDM (for a recent review on various 2HDM, see, e.g., [78]) to see whether this constraint can be avoided.

The lightest neutral component pseudoscalar A or CP-even state H in the inert 2HDM is stable and can act as a DM candidate, but it is highly restricted. The 2HDM itself can achieve a strong electroweak FOPT in the early universe [79, 80], so the extended real singlet scalar S can be independent of the FOPT. If so, the VEV of S field is zero at zero-temperature, and thus S serves as a DM candidate. For instance, Ref. [55] systematically studied the electroweak FOPT and the DM in the type-II 2HDM, taking the relevant constraints into consideration. It showed the surviving parameter space where the FOPT happens between the symmetric phase and the broken phase (with $v_s = 0$, and non-zero v_{h_1} and/or v_{h_2}), and the singlet field configuration keeps zero in evolution of the Universe. This strongly indicates that the singlet scalar may not be related to the transition temperature.

We focus on the dilution of DM density in this type-II 2HDM. The tree-level scalar potential is given as

$$\begin{aligned}
V_0^{2\text{HDM}+S} &= m_{11}^2(\Phi_1^\dagger\Phi_1) + m_{22}^2(\Phi_2^\dagger\Phi_2) - [m_{12}^2\Phi_1^\dagger\Phi_2 + h.c.] \\
&+ \frac{\lambda_1}{2}(\Phi_1^\dagger\Phi_1)^2 + \frac{\lambda_2}{2}(\Phi_2^\dagger\Phi_2)^2 + \frac{\lambda_3}{2}(\Phi_1^\dagger\Phi_1)(\Phi_2^\dagger\Phi_2) + \frac{\lambda_4}{2}(\Phi_1^\dagger\Phi_2)(\Phi_2^\dagger\Phi_1) \\
&+ [\frac{\lambda_5}{2}(\Phi_1^\dagger\Phi_2)^2 + h.c.] + \frac{1}{2}S^2(\kappa_1\Phi_1^\dagger\Phi_1 + \kappa_2\Phi_2^\dagger\Phi_2) + \frac{m_0}{2}S^2 + \frac{\lambda_S}{4!}S^4.
\end{aligned} \tag{4.1}$$

Here we parameterize the two Higgs-doublets in a similar way as in the xSM, assuming all parameters are real, and construct the one-loop effective potential using the OS-like scheme [55]. After spontaneous electroweak symmetry breaking, the scalar field S gets a mass

$$m_S^2 = m_0^2 + \frac{1}{2}\kappa_1 v^2 \cos^2 \beta + \frac{1}{2}\kappa_2 v^2 \sin^2 \beta, \quad (4.2)$$

where $v = \sqrt{v_{h_1}^2 + v_{h_2}^2} = 246$ GeV. As the DM candidate, its thermally averaged annihilation cross sections are given by [81]

$$\begin{aligned} \langle \sigma_{X\bar{X}} v_{\text{rel}} \rangle &= \sum_{\mathcal{H} \in \{h, H\}} \left| \frac{g_{\mathcal{H}SS} C_X^{\mathcal{H}}}{4m_S^2 - m_{\mathcal{H}}^2 + i\Gamma_{\mathcal{H}} m_{\mathcal{H}}} \right|^2 \frac{\Gamma_{\text{SM}}(\mathcal{H}^* \rightarrow X\bar{X})}{2m_S} \\ \langle \sigma_{H_i H_j} v_{\text{rel}} \rangle &= \frac{\beta(m_{H_i}, m_{H_j})}{32\pi(1 + \delta_{ij})m_S^2} \left| g_{H_i H_j SS} + \sum_{\mathcal{H} \in \{h, H\}} \frac{g_{\mathcal{H}SS} g_{\mathcal{H}H_i H_j}}{4m_S^2 - m_{\mathcal{H}}^2 + i\Gamma_{\mathcal{H}} m_{\mathcal{H}}} \right. \\ &\quad \left. + 2\delta_{\text{CP}} \frac{g_{H_i SS} g_{H_j SS}}{\frac{1}{2}(m_{H_i}^2 + m_{H_j}^2) - 2m_S^2} \right|^2, \end{aligned} \quad (4.3)$$

where $C_X^{\mathcal{H}}$ stands for the normalized coupling of \mathcal{H} to $X\bar{X}$, δ_{CP} is 0 for AA and H^+H^- and 1 for other cases, and

$$\beta(m_{H_i}, m_{H_j}) = \left(1 - \frac{m_{H_i}^2 + m_{H_j}^2}{2m_S^2} + \frac{(m_{H_i}^2 - m_{H_j}^2)^2}{16m_S^4} \right)^{\frac{1}{2}}. \quad (4.4)$$

The CP-even neutral Higgs couplings can be reorganized as

$$\begin{aligned} \lambda_h &= -\kappa_1 \sin \alpha \cos \beta + \kappa_2 \cos \alpha \sin \beta, \\ \lambda_H &= -\kappa_1 \cos \alpha \cos \beta + \kappa_2 \sin \alpha \sin \beta. \end{aligned} \quad (4.5)$$

Therefore we can choose the input model parameters as $\tan \beta$, $\sin(\beta - \alpha)$, m_H , m_{H^\pm} , m_{12} , m_0 , λ_h , and λ_H . In this way, m_0 is a free parameter which is independent of the phase transition properties, so the DM mass m_S can be large enough to enhance the freeze-out temperature T_f to above the transition temperature T_n .

In Fig. 7 we display T_c , T_n and T_f with a varying m_0 in the left panel, and the dilution factor d with a varying mixing parameter m_{12} in the right panel around the benchmark point [55]

$$\begin{aligned} \tan \beta &= 1.87, \quad \sin(\beta - \alpha) = 0.9991, \quad m_H = 387.97 \text{ GeV}, \quad m_{H^\pm} = 618.31 \text{ GeV}, \\ m_{12} &= 231.41 \text{ GeV}, \quad m_S = 501.7 \text{ GeV}, \quad \lambda_H = -0.129, \quad \lambda_S = 10.93 \end{aligned} \quad (4.6)$$

We see clearly that the transition temperatures T_c and T_n are independent of m_0 , and there is no upper bound on m_s . The light brown band indicates the possible range of T_f due to the variation of the parameter $x_f = m_S/T_f$ from 20 to 40 with the changing DM coupling. When $m_S > 2$ TeV, T_c becomes lower than T_f in the parameter space for this benchmark point. The right panel shows that the dilution factor increases with m_{12} decreasing, so does

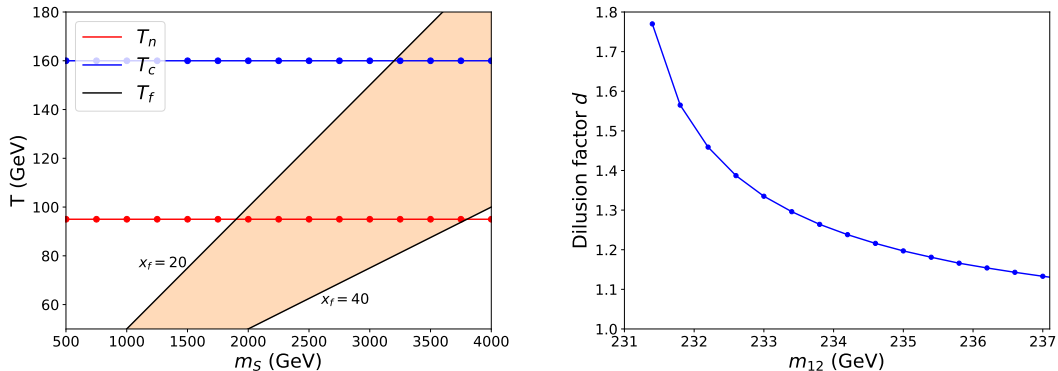


Figure 7. The critical temperature T_c , the nucleation temperature T_n and the freeze-out temperature T_f as functions of m_S (left), and the dilution factor f as a function of m_{12} (right) for the 2HDM+S.

the difference between T_c and T_n . The biggest dilution factor value can reach 1.77. If m_{12} further decreases, there is no more T_n , as shown in Fig. 3 for the xSM.

Note that when $T_n < T_f$, the value of T_f obtained from `MicrOmega` is not accurate, as mentioned in Sec. 2.3. When the DM deviates from the thermal equilibrium, the electroweak symmetry is still conserved. Thus, the DM mass appearing in the Boltzmann equation should be

$$m_S^2 = m_0^2 + [4\kappa_1 + 4\kappa_2 + \lambda_S] \frac{T^2}{24}, \quad (4.7)$$

instead of Eq. (4.2), where the second part is the thermal correction to the singlet in the situation of no mixing between the singlet and Higgs fields. The couplings of DM and mediated Higgs fields are also temperature dependent. For instance, the temperature dependent couplings in the xSM can be seen from Eq. (3.19). So the temperature dependent cross section indicates that $\langle v\sigma \rangle$ is very different from the result without thermal corrections, as well as the λ . Some dynamical reactions caused by the finite temperature correction may visibly affect the final DM relic density [53, 82–84]. These adjustments are beyond the scope of `MicrOmega`. For our case, we have seen in Fig. 1 that the impact on T_f is not dramatic. As far as the freeze-out temperature T_f is still larger than the transition temperature T_n , the dilution effect of FOPT will exist with same magnitude shown in the right panel of Fig. 7

5 Next-to-minimal supersymmetric standard model

In the singlet extension of the 2HDM, the strong FOPT can also be triggered by the broken singlet vacuum expectation value. A special realization of this FOPT case is the next-to-minimal supersymmetric standard model (NMSSM) [85], which is a popular scenario of low energy supersymmetry. Despite of null search results of superparticles at the LHC, so far the low energy supersymmetry still remains as a compelling BSM candidate (for recent reviews, see, e.g., [86, 87]). Besides addressing the baryon asymmetry and the DM issue as

well as the hierarchy problem of the electroweak scale [88], the low energy supersymmetry can give a joint explanation for the muon and electron $g - 2$ anomalies [89–91] (it can even marginally explain the CFD II measurement of the W-boson mass [92, 93]). The NMSSM introduces a SM gauge-singlet chiral superfield to generate the μ -term dynamically and the singlet scalar can couple with the Higgs doublets to sizably enhance the tree-level mass of the SM-like Higgs boson with no need of large radiative effects from heavy top-squarks. So from the point of 125 GeV Higgs boson mass, the NMSSM is more favored than the MSSM (minimal supersymmetric standard model) [94].

The NMSSM can be treated as a special case of the singlet extension of the 2HDM, where the strong FOPT is triggered by the broken singlet vacuum expectation value and hence relevant to the μ parameter (the higgsino mass).

In this model, assuming R-parity symmetry, the lightest neutralino is usually taken as the DM candidate, which is the mixing of neutral higgsinos, gauginos and singlino. Thus, the DM mass is bounded below by the smallest one among the higgsino mass μ , bino mass M_1 , wino mass M_3 and singlino mass $2\kappa v_S$. The annihilation channels are much more complex than in above models, which are dependent on the component of DM, and there may be also co-annihilations with sleptons or squarks. As studied in [95–99], to achieve a strong FOPT in the NMSSM, the μ parameter must be smaller than 1 TeV. As a result, the neutralino DM must be lighter than 1 TeV and the freeze-out temperature $T_f < 50$ GeV is lower than the nucleation temperature as in the xSM. In conclusion, the strong FOPT happens before the neutralino DM freeze-out, so the dilution of DM relic density can be neglected in the NMSSM.

6 Conclusions

We systematically analyzed the dilution of DM relic density caused by the FOPT in the singlet extension models, including the xSM, 2HDM+S and NMSSM. We found that in case of supercooling the released entropy can dilute the DM density to 1/3 at most. However, the singlet field configure in the xSM is relevant to the strength of the phase transition, which sets an upper limit of 600 GeV on the singlet DM mass and an upper limit of 30 GeV on the singlet DM freeze-out temperature. Meanwhile, the nucleation temperature is larger than 50 GeV from our scan. Thus, the strong FOPT happens before the singlet DM freeze-out and the dilution effect is negligible for the current DM density in the xSM. In the type-II 2HDM+S, the singlet scalar can be independent of the phase transition, so there is no upper bound on the singlet DM freeze-out temperature. As a result, the DM relic density, as well as the DM direct detection, can be affected by the FOPT in the type-II 2HDM+S. In the NMSSM with FOPT, the neutralino DM freeze-out temperature is lower than the nucleation temperature as in the xSM and thus the dilution of the DM relic density can be neglected.

Acknowledgments

We would like to thank Subhojit Roy for helpful communications. YZ thanks Institute of Theoretical Physics of Chinese Academy of Sciences (CAS) and YX thanks Zhengzhou University for hospitality during various stages of this work. This work was supported by the National Natural Science Foundation of China (NNSFC) under grant numbers 12105248, 11821505 and 12075300, by Peng-Huan-Wu Theoretical Physics Innovation Center under grant number 12047503, by a Key R&D Program of Ministry of Science and Technology of China under grant number 2017YFA0402204, by the Key Research Program of the Chinese Academy of Sciences under grant number XDPB15, by the CAS Center for Excellence in Particle Physics (CCEPP), and by Zhengzhou University Young Talent Program.

References

- [1] D. Kirzhnits and A. Linde, *Macroscopic consequences of the weinberg model*, *Physics Letters B* **42** (1972) 471–474.
- [2] K. Kajantie, M. Laine, K. Rummukainen and M. Shaposhnikov, *A non-perturbative analysis of the finite- t phase transition in $su(2) \times u(1)$ electroweak theory*, *Nuclear Physics B* **493** (1997) 413–438.
- [3] M. Trodden, *Electroweak baryogenesis*, *Rev. Mod. Phys.* **71** (Oct, 1999) 1463–1500.
- [4] J. M. Cline, *Baryogenesis*, in *Les Houches Summer School - Session 86: Particle Physics and Cosmology: The Fabric of Spacetime*, 9, 2006, [hep-ph/0609145](#).
- [5] G. A. White, *A Pedagogical Introduction to Electroweak Baryogenesis*. 2053-2571. Morgan and Claypool Publishers, 2016, [10.1088/978-1-6817-4457-5](#).
- [6] D. E. Morrissey and M. J. Ramsey-Musolf, *Electroweak baryogenesis*, *New J. Phys.* **14** (2012) 125003, [[1206.2942](#)].
- [7] A. Kosowsky, M. S. Turner and R. Watkins, *Gravitational waves from first-order cosmological phase transitions*, *Phys. Rev. Lett.* **69** (Oct, 1992) 2026–2029.
- [8] M. Kamionkowski, A. Kosowsky and M. S. Turner, *Gravitational radiation from first order phase transitions*, *Phys. Rev. D* **49** (1994) 2837–2851, [[astro-ph/9310044](#)].
- [9] PLANCK collaboration, P. A. R. Ade et al., *Planck 2015 results. XIII. Cosmological parameters*, *Astron. Astrophys.* **594** (2016) A13, [[1502.01589](#)].
- [10] PARTICLE DATA GROUP collaboration, R. L. Workman and Others, *Review of Particle Physics*, *PTEP* **2022** (2022) 083C01.
- [11] A. D. Sakharov, *Violation of cp -invariance, c -asymmetry, and baryon asymmetry of the universe*, in *In The Intermissions... Collected Works on Research into the Essentials of Theoretical Physics in Russian Federal Nuclear Center, Arzamas-16*, pp. 84–87. World Scientific, 1998.
- [12] B. Garbrecht, T. Prokopec and M. G. Schmidt, *Coherent baryogenesis*, *Phys. Rev. Lett.* **92** (Feb, 2004) 061303.
- [13] H. Davoudiasl, R. Kitano, G. D. Kribs, H. Murayama and P. J. Steinhardt, *Gravitational baryogenesis*, *Phys. Rev. Lett.* **93** (Nov, 2004) 201301.

- [14] J. D. Barrow, E. J. Copeland, E. W. Kolb and A. R. Liddle, *Baryogenesis in extended inflation. ii. baryogenesis via primordial black holes*, *Phys. Rev. D* **43** (Feb, 1991) 984–994.
- [15] A. Dolgov, K. Freese, R. Rangarajan and M. Srednicki, *Baryogenesis during reheating in natural inflation and comments on spontaneous baryogenesis*, *Phys. Rev. D* **56** (Nov, 1997) 6155–6165.
- [16] R. Rangarajan and D. V. Nanopoulos, *Inflationary baryogenesis*, *Phys. Rev. D* **64** (Aug, 2001) 063511.
- [17] A. G. Polnarev and M. Y. Khlopov, *The ERA of superheavy-particle dominance and big bang nucleosynthesis*, *Astronomicheskii Zhurnal* **59** (Feb., 1982) 15–19.
- [18] G. L. Alberghi, R. Casadio and A. Tronconi, *Radion induced spontaneous baryogenesis*, *Modern Physics Letters A* **22** (2007) 339–346.
- [19] G. W. Anderson and L. J. Hall, *Electroweak phase transition and baryogenesis*, *Phys. Rev. D* **45** (Apr, 1992) 2685–2698.
- [20] P. Huet and A. E. Nelson, *Electroweak baryogenesis in supersymmetric models*, *Phys. Rev. D* **53** (Apr, 1996) 4578–4597.
- [21] T. Ghosh, H.-K. Guo, T. Han and H. Liu, *Electroweak phase transition with an $SU(2)$ dark sector*, *Journal of High Energy Physics* **2021** (jul, 2021) .
- [22] T. Prokopec, J. Rezaeck and B. Ś wieżewska, *Gravitational waves from conformal symmetry breaking*, *Journal of Cosmology and Astroparticle Physics* **2019** (feb, 2019) 009–009.
- [23] I. Baldes and C. Garcia-Cely, *Strong gravitational radiation from a simple dark matter model*, *Journal of High Energy Physics* **2019** (may, 2019) .
- [24] Z. Wang, X. Zhu, E. E. Khoda, S.-C. Hsu, N. Konstantinidis, K. Li et al., *Study of Electroweak Phase Transition in Exotic Higgs Decays at the CEPC*, in *2022 Snowmass Summer Study*, 3, 2022, [2203.10184](#).
- [25] M. Maggiore, *Gravitational wave experiments and early universe cosmology*, *Phys. Rept.* **331** (2000) 283–367, [[gr-qc/9909001](#)].
- [26] D. J. Weir, *Gravitational waves from a first order electroweak phase transition: a brief review*, *Phil. Trans. Roy. Soc. Lond. A* **376** (2018) 20170126, [[1705.01783](#)].
- [27] T. Alanne, T. Hügler, M. Platscher and K. Schmitz, *A fresh look at the gravitational-wave signal from cosmological phase transitions*, *JHEP* **03** (2020) 004, [[1909.11356](#)].
- [28] LIGO SCIENTIFIC, VIRGO collaboration, B. P. Abbott et al., *Observation of Gravitational Waves from a Binary Black Hole Merger*, *Phys. Rev. Lett.* **116** (2016) 061102, [[1602.03837](#)].
- [29] P. Amaro-Seoane, H. Audley, S. Babak, J. Baker, E. Barausse, P. Bender et al., *Laser Interferometer Space Antenna*, *arXiv e-prints* (Feb., 2017) arXiv:1702.00786, [[1702.00786](#)].
- [30] W.-R. Hu and Y.-L. Wu, *The Taiji Program in Space for gravitational wave physics and the nature of gravity*, *National Science Review* **4** (10, 2017) 685–686, [<https://academic.oup.com/nsr/article-pdf/4/5/685/31566708/nwx116.pdf>].
- [31] PLANCK collaboration, N. Aghanim et al., *Planck 2018 results. VI. Cosmological parameters*, *Astron. Astrophys.* **641** (2020) A6, [[1807.06209](#)].
- [32] S. Chatterjee, A. Das, T. Samui and M. Sen, *Mixed wimp-axion dark matter*, *Phys. Rev. D* **100** (Dec, 2019) 115050.

- [33] S. Kanemura, S. Matsumoto, T. Nabeshima and N. Okada, *Can wimp dark matter overcome the nightmare scenario?*, *Phys. Rev. D* **82** (Sep, 2010) 055026.
- [34] E. M. Dolle and S. Su, *Inert dark matter*, *Phys. Rev. D* **80** (Sep, 2009) 055012.
- [35] A. Liu, Z.-L. Han, Y. Jin and F.-X. Yang, *Leptogenesis and dark matter from a low scale seesaw mechanism*, *Phys. Rev. D* **101** (May, 2020) 095005.
- [36] P.-H. Gu, M. Hirsch, U. Sarkar and J. W. F. Valle, *Neutrino masses, leptogenesis, and dark matter in a hybrid seesaw model*, *Phys. Rev. D* **79** (Feb, 2009) 033010.
- [37] F. Bezrukov, H. Hettmansperger and M. Lindner, *keV sterile neutrino dark matter in gauge extensions of the standard model*, *Phys. Rev. D* **81** (Apr, 2010) 085032.
- [38] T. Tsuyuki, *Neutrino masses, leptogenesis, and sterile neutrino dark matter*, *Phys. Rev. D* **90** (Jul, 2014) 013007.
- [39] R. T. Co, L. J. Hall and K. Harigaya, *Qcd axion dark matter with a small decay constant*, *Phys. Rev. Lett.* **120** (May, 2018) 211602.
- [40] O. Erken, P. Sikivie, H. Tam and Q. Yang, *Axion dark matter and cosmological parameters*, *Phys. Rev. Lett.* **108** (Feb, 2012) 061304.
- [41] M. Kawasaki, K. Saikawa and T. Sekiguchi, *Axion dark matter from topological defects*, *Phys. Rev. D* **91** (Mar, 2015) 065014.
- [42] XENON COLLABORATION collaboration, E. Aprile, J. Aalbers, F. Agostini, M. Alfonsi, L. Althueser, F. D. Amaro et al., *Search for inelastic scattering of wimp dark matter in xenon1t*, *Phys. Rev. D* **103** (Mar, 2021) 063028.
- [43] M. A. Fedderke, P. W. Graham and S. Rajendran, *Axion dark matter detection with cmb polarization*, *Phys. Rev. D* **100** (Jul, 2019) 015040.
- [44] XENON COLLABORATION collaboration, E. Aprile, J. Aalbers, F. Agostini, M. Alfonsi, F. D. Amaro, M. Anthony et al., *First dark matter search results from the xenon1t experiment*, *Phys. Rev. Lett.* **119** (Oct, 2017) 181301.
- [45] M. Dine, L. Randall and S. Thomas, *Baryogenesis from flat directions of the supersymmetric standard model*, *Nuclear Physics B* **458** (jan, 1996) 291–323.
- [46] T. Banks, D. B. Kaplan and A. E. Nelson, *Cosmological implications of dynamical supersymmetry breaking*, *Physical Review D* **49** (jan, 1994) 779–787.
- [47] A. Mégevand, *First-order cosmological phase transitions in the radiation-dominated era*, *Physical Review D* **69** (2004) 103521.
- [48] A. Megevand and A. D. Sanchez, *Supercooling and phase coexistence in cosmological phase transitions*, *Physical Review D* **77** (2008) 063519.
- [49] C. Wainwright and S. Profumo, *Impact of a strongly first-order phase transition on the abundance of thermal relics*, *Physical Review D* **80** (2009) 103517.
- [50] D. Chung, A. Long and L.-T. Wang, *Probing the cosmological constant and phase transitions with dark matter*, *Physical Review D* **84** (2011) 043523.
- [51] A. Azatov, M. Vanvlasselaer and W. Yin, *Dark matter production from relativistic bubble walls*, *Journal of High Energy Physics* **2021** (2021) 1–31.
- [52] A. Azatov, G. Barni, S. Chakraborty, M. Vanvlasselaer and W. Yin, *Ultra-relativistic bubbles*

from the simplest higgs portal and their cosmological consequences, *arXiv preprint arXiv:2207.02230* (2022) .

- [53] L. Bian and Y.-L. Tang, *Thermally modified sterile neutrino portal dark matter and gravitational waves from phase transition: The freeze-in case*, *Journal of High Energy Physics* **2018** (2018) 1–29.
- [54] L. Bian and X. Liu, *Two-step strongly first-order electroweak phase transition modified fimp dark matter, gravitational wave signals, and the neutrino mass*, *Physical Review D* **99** (2019) 055003.
- [55] X.-F. Han, L. Wang and Y. Zhang, *Dark matter, electroweak phase transition, and gravitational waves in the type II two-Higgs-doublet model with a singlet scalar field*, *Phys. Rev. D* **103** (2021) 035012, [[2010.03730](#)].
- [56] N. Blinov, S. Profumo and T. Stefaniak, *The electroweak phase transition in the inert doublet model*, *Journal of Cosmology and Astroparticle Physics* **2015** (2015) 028.
- [57] K. L. McDonald et al., *Secluded dark matter coupled to a hidden cft*, *Journal of High Energy Physics* **2012** (2012) .
- [58] A. D. Linde, *Decay of the false vacuum at finite temperature*, *Nuclear Physics B* **216** (1983) 421–445.
- [59] V. Rubakov, *Classical theory of gauge fields*. Princeton University Press, 2009.
- [60] M. Quiros, *Finite temperature field theory and phase transitions, Proceedings, Summer school in high-energy physics and cosmology: Trieste, Italy 1999* (1998) 187–259.
- [61] B. W. Lee and S. Weinberg, *Cosmological lower bound on heavy-neutrino masses*, *Phys. Rev. Lett.* **39** (Jul, 1977) 165–168.
- [62] S. Weinberg, *Cosmology*. OUP Oxford, 2008.
- [63] B.-L. Young, *A survey of dark matter and related topics in cosmology*, *Frontiers of Physics* **12** (2017) 1–219.
- [64] G. Belanger, F. Boudjema, A. Pukhov and A. Semenov, *Micromegas: A program for calculating the relic density in the mssm*, *Computer Physics Communications* **149** (2002) 103–120.
- [65] F. Ambroggi, C. Arina, M. Backovic, J. Heisig, F. Maltoni, L. Mantani et al., *MadDM v.3.0: a Comprehensive Tool for Dark Matter Studies*, *Phys. Dark Univ.* **24** (2019) 100249, [[1804.00044](#)].
- [66] J. M. Cline, K. Kainulainen, P. Scott and C. Weniger, *Update on scalar singlet dark matter*, *Phys. Rev. D* **88** (2013) 055025, [[1306.4710](#)].
- [67] P. Gondolo and G. Gelmini, *Cosmic abundances of stable particles: Improved analysis*, *Nucl. Phys. B* **360** (1991) 145–179.
- [68] J. Elias-Miro, J. Espinosa and T. Konstandin, *Taming infrared divergences in the effective potential*, *Journal of High Energy Physics* **2014** (2014) 1–27.
- [69] J. Braathen and M. D. Goodsell, *Avoiding the goldstone boson catastrophe in general renormalisable field theories at two loops*, *Journal of High Energy Physics* **2016** (2016) 1–41.
- [70] P. Athron, C. Balazs, A. Fowlie, L. Morris, G. White and Y. Zhang, *How arbitrary are perturbative calculations of the electroweak phase transition?*, [2208.01319](#).

- [71] D. Curtin, P. Meade and H. Ramani, *Thermal resummation and phase transitions*, *The European Physical Journal C* **78** (2018) 1–29.
- [72] E. Senaha, *Symmetry restoration and breaking at finite temperature: an introductory review*, *Symmetry* **12** (2020) 733.
- [73] R. R. Parwani, *Resummation in a hot scalar field theory*, *Phys. Rev. D* **45** (1992) 4695, [[hep-ph/9204216](#)].
- [74] C. L. Wainwright, *Cosmotransitions: Computing cosmological phase transition temperatures and bubble profiles with multiple fields*, *Computer Physics Communications* **183** (2012) 2006–2013.
- [75] P. Athron, C. Balázs, A. Fowlie and Y. Zhang, *PhaseTracer: tracing cosmological phases and calculating transition properties*, *Eur. Phys. J. C* **80** (2020) 567, [[2003.02859](#)].
- [76] P. Athron, J. M. Cornell, F. Kahlhoefer, J. Mckay, P. Scott and S. Wild, *Impact of vacuum stability, perturbativity and XENON1T on global fits of \mathbb{Z}_2 and \mathbb{Z}_3 scalar singlet dark matter*, *Eur. Phys. J. C* **78** (2018) 830, [[1806.11281](#)].
- [77] V. Vaskonen, *Electroweak baryogenesis and gravitational waves from a real scalar singlet*, *Physical Review D* **95** (2017) 123515.
- [78] L. Wang, J. M. Yang and Y. Zhang, *Two-Higgs-doublet models in light of current experiments: a brief review*, [2203.07244](#).
- [79] W. Su, A. G. Williams and M. Zhang, *Strong first order electroweak phase transition in 2HDM confronting future Z & Higgs factories*, *JHEP* **04** (2021) 219, [[2011.04540](#)].
- [80] L. Wang, *Inflation, electroweak phase transition, and Higgs searches at the LHC in the two-Higgs-doublet model*, [2105.02143](#).
- [81] A. Drozd, B. Grzadkowski, J. F. Gunion and Y. Jiang, *Extending two-Higgs-doublet models by a singlet scalar field - the Case for Dark Matter*, *JHEP* **11** (2014) 105, [[1408.2106](#)].
- [82] T. Cohen, D. E. Morrissey and A. Pierce, *Changes in Dark Matter Properties After Freeze-Out*, *Phys. Rev. D* **78** (2008) 111701, [[0808.3994](#)].
- [83] M. J. Baker, M. Breitbach, J. Kopp and L. Mittnacht, *Dynamic Freeze-In: Impact of Thermal Masses and Cosmological Phase Transitions on Dark Matter Production*, *JHEP* **03** (2018) 114, [[1712.03962](#)].
- [84] W. Chao, X.-F. Li and L. Wang, *Filtered pseudo-scalar dark matter and gravitational waves from first order phase transition*, *JCAP* **06** (2021) 038, [[2012.15113](#)].
- [85] U. Ellwanger, C. Hugonie and A. M. Teixeira, *The Next-to-Minimal Supersymmetric Standard Model*, *Phys. Rept.* **496** (2010) 1–77, [[0910.1785](#)].
- [86] F. Wang, W. Wang, J. Yang, Y. Zhang and B. Zhu, *Low Energy Supersymmetry Confronted with Current Experiments: An Overview*, *Universe* **8** (2022) 178, [[2201.00156](#)].
- [87] H. Baer, V. Barger, S. Salam, D. Sengupta and K. Sinha, *Status of weak scale supersymmetry after LHC Run 2 and ton-scale noble liquid WIMP searches*, *Eur. Phys. J. ST* **229** (2020) 3085–3141, [[2002.03013](#)].
- [88] E. Witten, *Mass hierarchies in supersymmetric theories*, *Physics Letters B* **105** (1981) 267–271.
- [89] S. Li, Z. Li, F. Wang and J. M. Yang, *Explanation of electron and muon $g - 2$ anomalies in AMSB*, [2205.15153](#).

- [90] S. Li, Y. Xiao and J. M. Yang, *Can electron and muon $g - 2$ anomalies be jointly explained in SUSY?*, *Eur. Phys. J. C* **82** (2022) 276, [[2107.04962](#)].
- [91] J. Cao, Y. He, J. Lian, D. Zhang and P. Zhu, *Electron and muon anomalous magnetic moments in the inverse seesaw extended NMSSM*, *Phys. Rev. D* **104** (2021) 055009, [[2102.11355](#)].
- [92] J. M. Yang and Y. Zhang, *Low energy SUSY confronted with new measurements of W -boson mass and muon $g-2$* , *Science Bulletin* **67** (2022) 1430–1436, [[2204.04202](#)].
- [93] T.-P. Tang, M. Abdughani, L. Feng, Y.-L. S. Tsai, J. Wu and Y.-Z. Fan, *NMSSM neutralino dark matter for W -boson mass and muon $g - 2$ and the promising prospect of direct detection*, [2204.04356](#).
- [94] J.-J. Cao, Z.-X. Heng, J. M. Yang, Y.-M. Zhang and J.-Y. Zhu, *A SM-like Higgs near 125 GeV in low energy SUSY: a comparative study for MSSM and NMSSM*, *JHEP* **03** (2012) 086, [[1202.5821](#)].
- [95] W. Huang, Z. Kang, J. Shu, P. Wu and J. M. Yang, *New insights in the electroweak phase transition in the NMSSM*, *Phys. Rev. D* **91** (2015) 025006, [[1405.1152](#)].
- [96] L. Bian, H.-K. Guo and J. Shu, *Gravitational Waves, baryon asymmetry of the universe and electric dipole moment in the CP-violating NMSSM*, *Chin. Phys. C* **42** (2018) 093106, [[1704.02488](#)].
- [97] P. Athron, C. Balazs, A. Fowlie, G. Pozzo, G. White and Y. Zhang, *Strong first-order phase transitions in the NMSSM — a comprehensive survey*, *JHEP* **11** (2019) 151, [[1908.11847](#)].
- [98] A. Chatterjee, A. Datta and S. Roy, *Electroweak phase transition in the Z_3 -invariant NMSSM: Implications of LHC and Dark matter searches and prospects of detecting the gravitational waves*, *JHEP* **06** (2022) 108, [[2202.12476](#)].
- [99] S. Baum, M. Carena, N. R. Shah, C. E. M. Wagner and Y. Wang, *Nucleation is more than critical: A case study of the electroweak phase transition in the NMSSM*, *JHEP* **03** (2021) 055, [[2009.10743](#)].